On the Evolution of the *QE II* Storm. I: Synoptic Aspects

JOHN R. GYAKUM[1]

Department of Meteorology and Physical Oceanography, Massachusetts Institute of Technology, Cambridge, MA 02139

(Manuscript received 21 June 1982, in final form 26 October 1982)

ABSTRACT

The hurricane-force winds and heavy seas which battered the liner *Queen Elizabeth II* on 10 and 11 September 1978 were associated with an extreme example of a meteorological "bomb" as defined by Sanders and Gyakum. Despite the existence of surface buoys, and the relatively high density of mobile ships in the North Atlantic, real-time weather analyses, subjective forecasts, and numerical prognoses all erred in the intensity and track of this storm. In this study, deficiencies in the real-time surface analysis were compensated for by the addition of Seasat-A surface wind fields and previously-discarded conventional ship reports. This paper examines the synoptic aspects of this case with emphasis on physical mechanisms most likely responsible for the development.

The cyclone originated as a shallow barocline disturbance west of Atlantic City, New Jersey, and explosive deepening (~60 mb/24 h) commenced once the storm moved offshore, and in association with cumulus convection adjacent to the storm center. The hurricane-force winds, a deep tropospheric warm core, and a clear eye-like center, all characteristics of a tropical cycline, were associated with this storm at 1200 GMT 10 September.

A diagnostic assessment of baroclinic forcing reveals that, although the cyclone formed on the anticyclonic shear side of the 500 mb flow, a shallow lower tropospheric layer of cyclonic thermal vorticity advection existed over the surface cyclone center. Calculations using a diagnostic, adiabatic, inviscid quasi-geostrophic model, which can approximately replicate the shallow baroclinic structure of this cyclone, yield instantaneous vertical motion and deepening rates far less than those observed. It is suggested that the convection associated with this cyclone during its explosive deepening played a substantial additional role, as in tropical cyclone formation, in this cyclone's evolution.

1. Introduction

The meteorological conditions associated with the explosive intensification of the September 1978 cyclone which battered the liner *Queen Elizabeth II* (*QE II*), and in which the dragger *Captain Cosmo* was lost (NOAA, 1979) constitute the prime topic of this paper. We will see that tropical cyclone characteristics of wind, deep convection and a clear, warm eyelike center were all associated with this cyclone, even though this cyclogenesis occurred just north of 40°N in the western Atlantic Ocean. Fig. 1 shows the extreme horizontal pressure contrasts experienced by the freighter *Euroliner* as it passed through the mature storm's center on 10 September. The data contained in this study reveal this initially shallow surface low to have intensified nearly 60 mb in 24 h, thus qualifying it as an extreme case of a "bomb" as defined by Sanders and Gyakum (1980, hereafter referred to as SG).

The numerical prognoses of both the National Meteorological Center (NMC) and Fleet Numerical Weather Central (FNWC) missed virtually all of this intensification. The addition of conventional ship reports, available in real time, and of Seasat-A surface wind reports helped to compensate for deficiencies in NMC's real-time analysis of this case, so that we will be able to see unusually detailed fields of wind and mass in this "bomb." That such a well-documented explosively-developing extratropical storm contained important similarities to that of a tropical cyclone and that its intensification was missed by the operational numerical models demand that further study be undertaken.

This paper details the synoptic aspects of the explosive cyclogenesis, while a companion paper examines the three-dimensional dynamic and thermodynamic storm structure, and why such explosive development occurred. Section 2 describes the data set used to document this case. The mesoscale and synoptic-scale conditions surrounding the cyclone will be discussed in Section 3. Operational numerical model performance will be discussed in Section 4, while Section 5 examines the vertical motions and quasi-geostrophic forcing associated with this cyclone. Results are discussed and conclusions presented in Section 6.

2. Data base

Aside from the surface data commonly available in real time (Service A hourlies, Service C 6-hourly

[1] Current Affiliation: Department of Atmospheric Sciences, University of Illinois, Urbana, IL 61801.

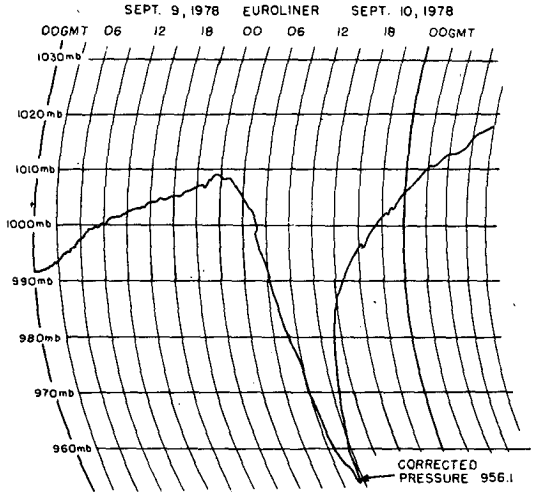

FIG. 1. *Euroliner* barograph trace for 9–10 September 1978.

synoptic land and ship reports, and NOAA data buoys), additional ship reports, along with barograms and copies of weather logs, were obtained from the National Climatic Center (NCC). The reports were supplemented by the Department of the Navy synoptic data file, the NMC surface data file, and ship weather logs and barograms furnished by the British Meteorological Office.

This study was aided by the availability of a wealth of surface wind reports derived from the Seasat-A satellite scatterometer system (SASS), which is a microwave radar, the characteristics of which are described in AAAS (1979). The wind data are available in the form of: the latitude and longitude of the observation and up to four wind speeds and four directions per observation. The wind speeds are all within 1 m s^{-1} of each other for each set of four readings. However, the ambiguity lies in the wind direction, which varies widely for a given observation. The selection of the "correct" wind direction has been performed subjectively for this case, and was based upon consistency with the nearby ship wind reports and *a priori* knowledge of the sea-level pressure field. Several hundred reports of these wind vector sets exist for each time and region of interest. The wind data are derived from orbits 1066 and 1080 of Seasat, the measurements of which correspond to within 55 minutes of the desired synoptic time. An appropriate time-space correction was applied to each observation.

Upper-level data were obtained from the NMC data file. Included are land and weather ship-based radiosonde data, commercial and military aircraft wind, temperature and height information, along with NOAA's geostationary (GOES-east) satellite temperature profiles. A set of GOES-east satellite cloud-top winds was furnished by the Space Science and Engineering Center at the University of Wisconsin.

GOES-east satellite visible and infrared images were obtained from the Satellite Data Services Division of the National Climatic Center (NCC) in Washington, D.C. Visible and infrared imagery of much higher horizontal resolution were obtained from the polar-orbiting Defense Meteorological Satellite.

Radar data were obtained from NCC in the form of nationwide summary charts of precipitation echoes, data sheets containing observations at individual radar stations, and film records of the actual plan position indicator (PPI). The individual stations used in this study are Atlantic City, New Jersey; New York, New York; Patuxent River, Maryland; and Chatham, Massachusetts; the locations of which are indicated in Fig. 2.

3. Mesoscale and synoptic overview

Fig. 3 shows mesoscale surface charts for 0000 and 0600 GMT 9 September 1978. At the former time, a surface front extended southeastward from the Great Lakes to Atlantic City, New Jersey. This frontal system separated an area of anomalously warm air prevalent in the southwestern Great Lakes from a relatively cool surface ridge centered over southeastern New York. This general pattern persisted for much of the month (Taubensee, 1978). Horizontal temperature contrasts in the frontal zone were in excess of 8°C/100 km. At this time, an incipient cy-

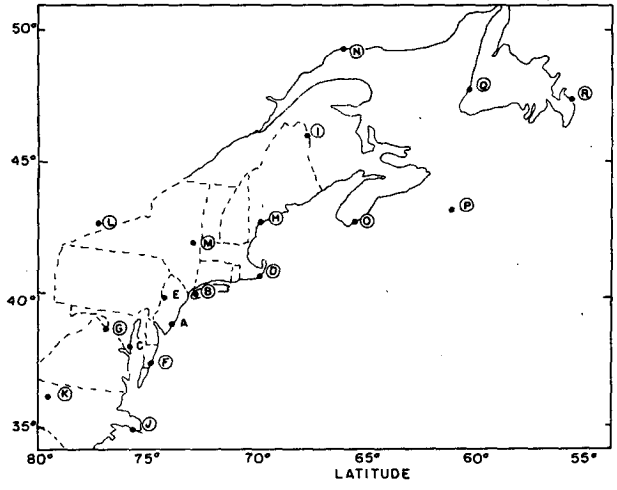

FIG. 2. Geographical locator map, in which circled letters represent radiosonde stations. The set of stations includes those mentioned in the text, plus radiosonde stations. International identifier numbers follow, where applicable: A–Atlantic City, NJ-72407; B–Fort Totton/New York, NY-74486; C–Patuxent River, MD-72404; D–Chatham, MA-74494; E–Trenton, NJ; F–Wallops Island, VA-72402; G–Dulles International, VA-72403; H–Portland, ME-72606; I–Caribou, ME-72712; J–Cape Hatteras, NC-72304; K–Greensboro, NC-72317; L–Buffalo, NY-72528; M–Albany, NY-72518; N–Sept Iles, Quebec-72811; O–Shelburne, Nova Scotia-74399; P–Sable Island, NS-72600; Q–Stephenville, Newfoundland-72815; R–St. John's, Newfoundland-72801.

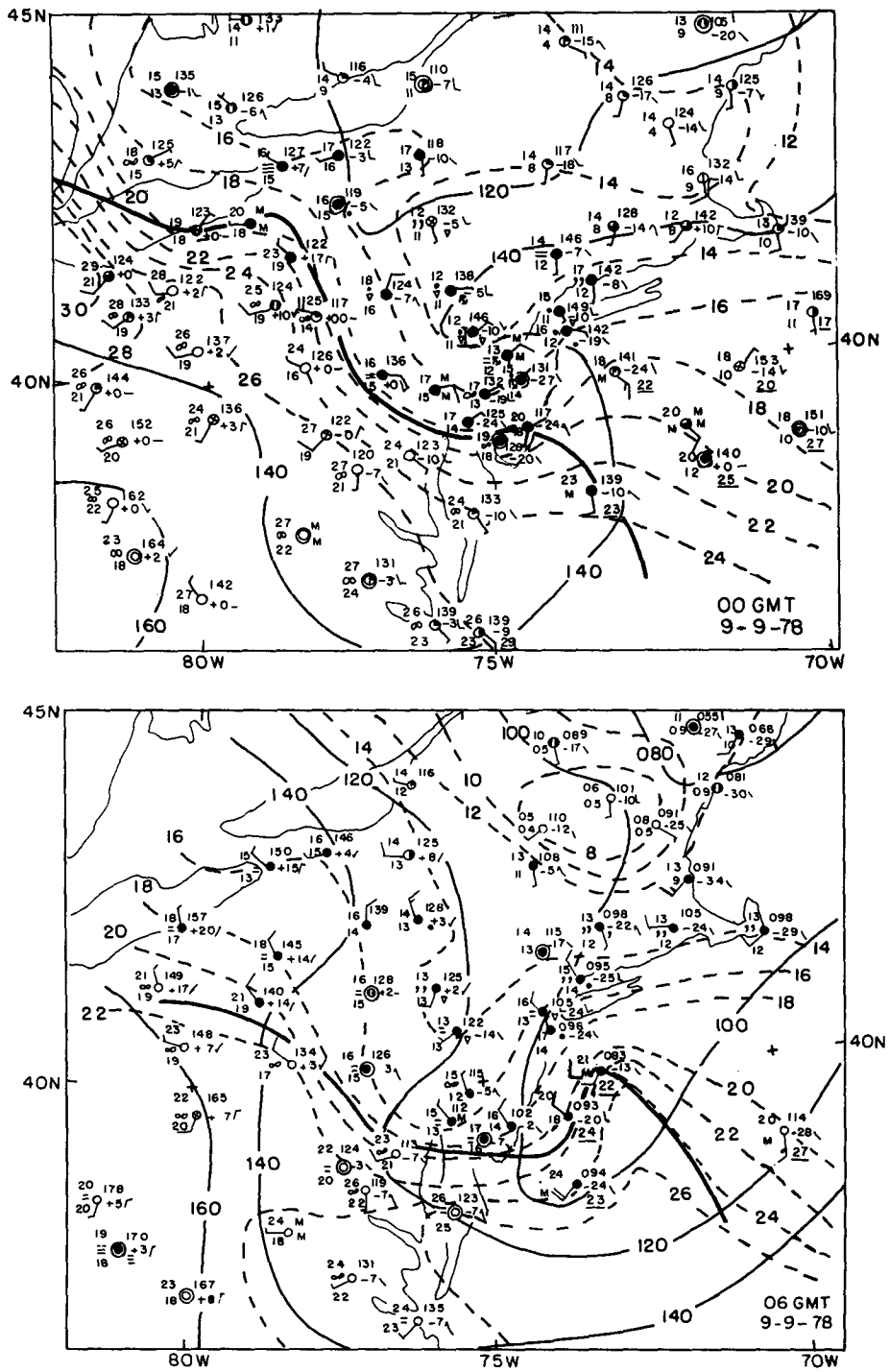

FIG. 3. Surface sectional plots in conventional format for 0000 and 0600 GMT 9 September 1978. Times appear in the lower right corner of each part of the figure. Temperatures are in °C, are analyzed in dashed lines, and winds are plotted in kt [1 kt = 0.515 m s^{-1}, thus pennant = 50 knots ≈ 25 m s^{-1}, full (half) barb = 10 (5) knots ≈ 5 (2.5 m s^{-1}]. Sea-level isobars (mb) are given by solid lines. Surface front is shown by heavy solid line. SST's, where appropriate, are underlined.

clonic circulation center appeared about 20 km west of Atlantic City, New Jersey. Note the relatively strong pressure falls (>2 mb/3 h) along the New Jersey coast, and the associated strong low-level warm advection in this region. Precipitation was confined to the north of the surface trough in the form of thunderstorms with 13 km maximum cloud tops and echo intensities corresponding to rainfall rates of 50–100

mm h^{-1}, as shown in the 2335 GMT radar summary (Fig. 4). By 0600 GMT the intensifying low (1008 mb) had moved northeastward offshore to just northwest of the NOAA buoy while the convective cells moved rapidly southeastward.

At this time, the developing cyclone was in the relatively clear air 60 km to the northwest of a rapidly developing convective cloud cluster, which fit Maddox's (1980) criteria for a mesoscale convective complex (MCC). This MCC and the surface cyclone center are shown in the infrared M_B-enhanced satellite image (Fig. 5). This enhancement, used by the National Environmental Satellite Service to indicate narrow ranges of cloud-top temperatures below −32°C, is described by Corbell *et al.* (1976). The MCC can be traced back in time to a few developing cells in east-central Pennsylvania at 0000 GMT on the 9th and is seen as the small area of thundershowers with 10 km maximum tops in the 0335 GMT radar summary (Fig. 4). The horizontal area of cold (≤−32°C) cloud tops of the incipient MCC had increased from 2500 km^2 at 0330 GMT to 105 000 km^2 at 0600 GMT. The M_B enhancement shows cloud tops extending up to 170 mb (−63°C). The MCC traveled an average of 23 m s^{-1} to the east-southeast, with a steering level of ~700 mb, and apparently moved independently of the east-northeastward moving surface cyclone. It reached a maximum size of 420 000 km^2 at 1000 GMT.

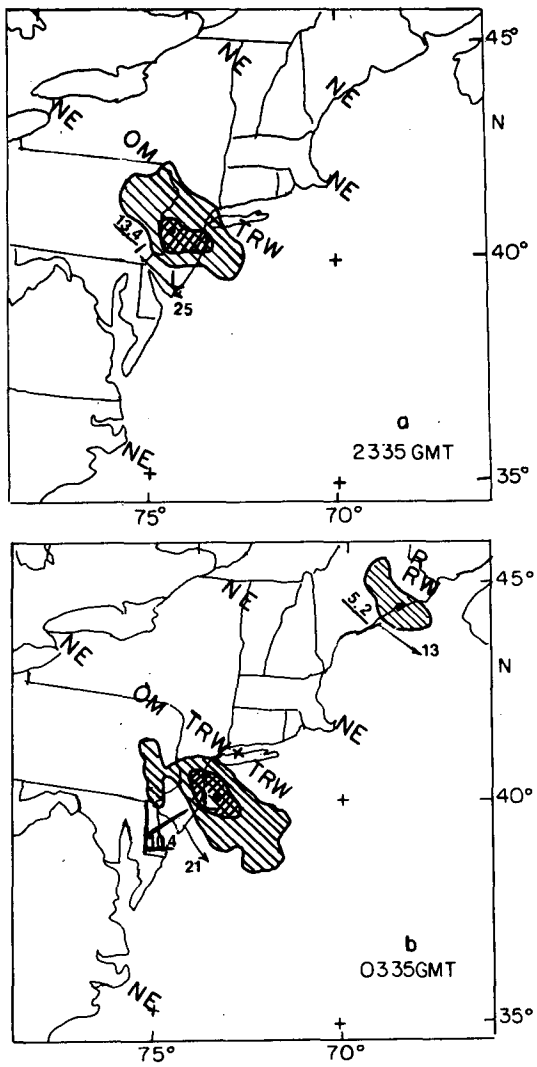

FIG. 4. Conventional radar summaries valid (a) 2335 GMT 8 September 1978 and (b) 0335 GMT 9 September 1978. Position of the surface cyclone is indicated with an "L." Maximum cloud top heights are indicated by underlined numbers (km), while cell movement is indicated by arrows with speeds (m s^{-1}).

The upper-level charts for 0000 GMT on the 9th are shown in Fig. 6. The most noteworthy feature is the rapidity with which the surface trough disappears with height. No associated trough exists at either the 500 mb or 250 mb levels. In fact, cyclonic relative vorticity in the Wallops–Fort Totten–Dulles triangle (indicated by WAL, JFK, and IAD in Fig. 6) is confined to levels below 890 mb. Cold high-tropopause air, which is characteristic of a subtropical atmosphere, is directly over the surface cyclone.

Once offshore, the cyclone assumed a more eastward track at an increased speed averaging 18 m s^{-1} between 0600 and 1200 GMT. Fig. 7 shows the time section of buoy observations at 40.1°N, 73.0°W, and at 40.8°N, 68.5°W. This deepening low clearly passed just to the north of the first buoy prior to 0700 GMT, and to the south of the second buoy between 1200 and 1300 GMT.

The storm continued on its eastward path and by 1200 GMT on the 9th had deepened to 1004 mb, as is shown in Fig. 8. The sea-level pressure (Fig. 9) analysis has been reinforced by the addition of Seasat surface winds.

The Seasat set adds considerable detail to the information given by the existing array of ship reports and buoy observations. This surface wind set was used to construct an isotach–isogon analysis from which divergences and relative vorticities have been computed on a one-degree latitude by one-degree longitude grid. This same procedure is used for 1200 GMT 10 September when Seasat coverage also exists. A rather high relative vorticity value of 17×10^{-5} s^{-1} is computed at 1200 GMT 9 September at the surface cyclone center.

The surface system at this time was still quite shallow, as no associated trough is detected at 250 mb. Fig. 9 also shows the surface low to be southwest of the maximum mean tropospheric virtual temperature gradient. Wind reports from commercial aircraft at ~250 mb supplement the radiosonde information. Winds are assumed to be geostropic at this level and, with the subtraction of the corresponding 1000 mb geostrophic wind vector based upon the sea-level pressure analyses, a thermal wind is computed for each data point. This procedure is the basis for the mean tropospheric temperature analysis in Fig. 9.

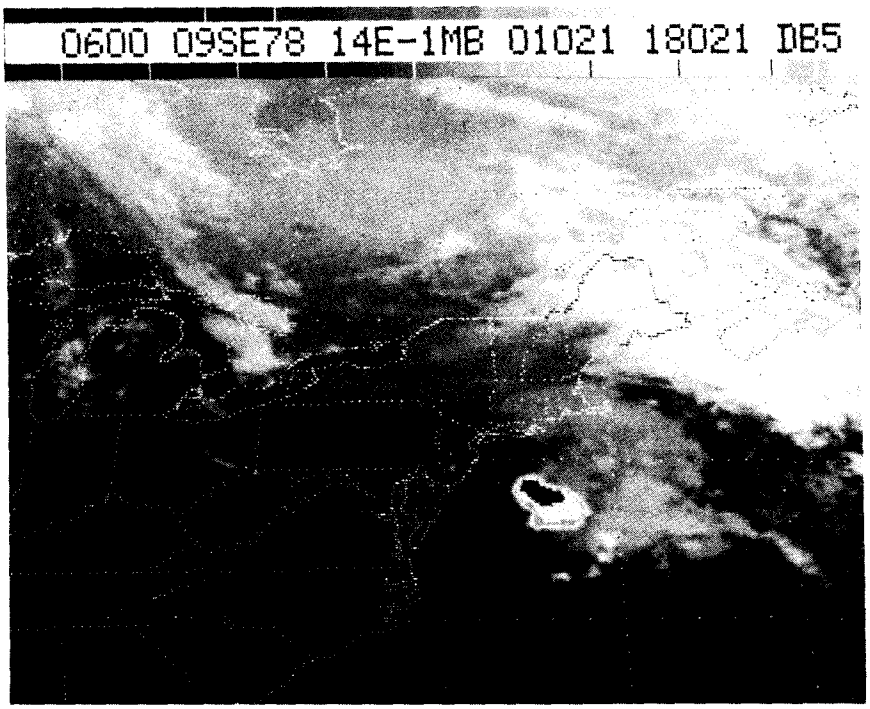

FIG. 5. GOES-east M_B-enhanced satellite image for 0600 GMT 9 September 1978. Circle indicates the surface cyclone center, which is located just south of Long Island at 40.1°N, 73.0°W.

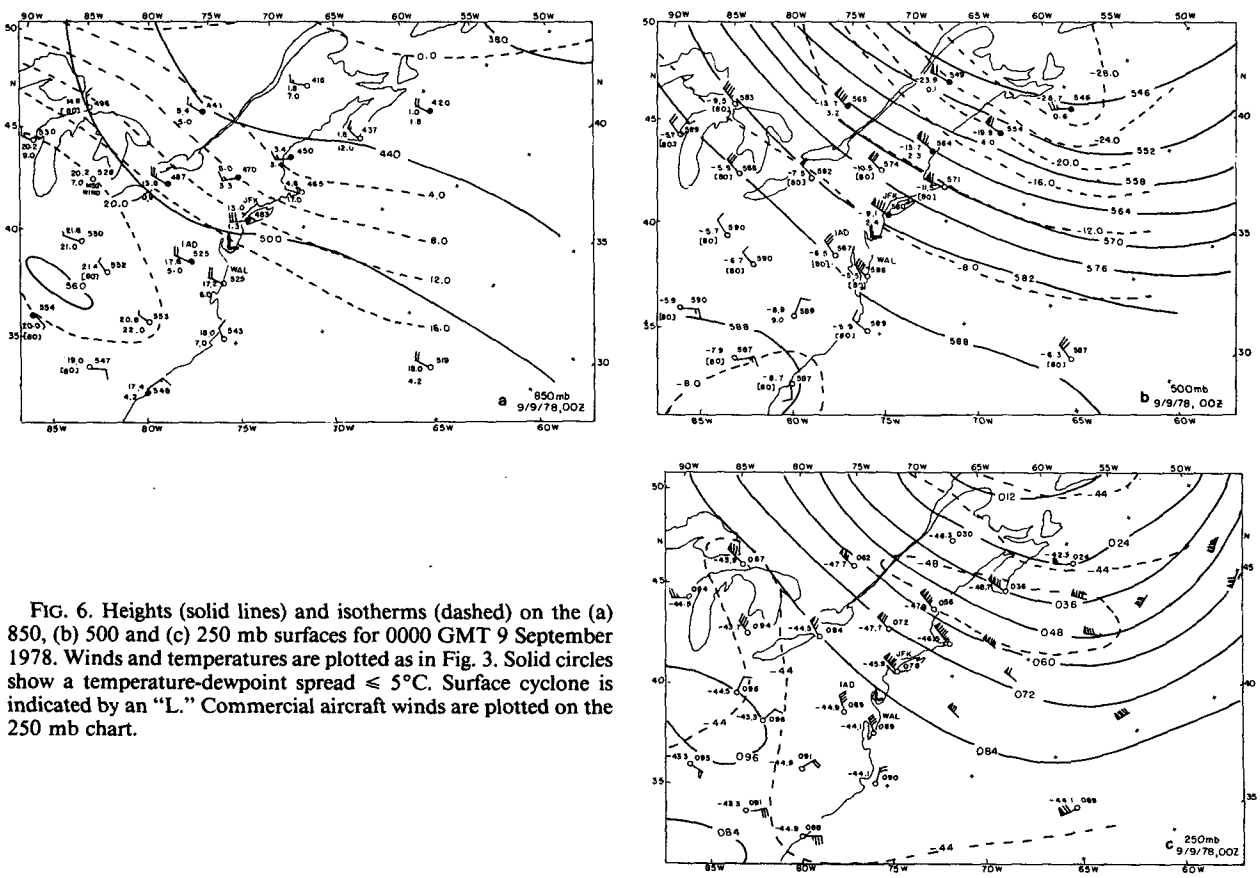

FIG. 6. Heights (solid lines) and isotherms (dashed) on the (a) 850, (b) 500 and (c) 250 mb surfaces for 0000 GMT 9 September 1978. Winds and temperatures are plotted as in Fig. 3. Solid circles show a temperature-dewpoint spread ≤ 5°C. Surface cyclone is indicated by an "L." Commercial aircraft winds are plotted on the 250 mb chart.

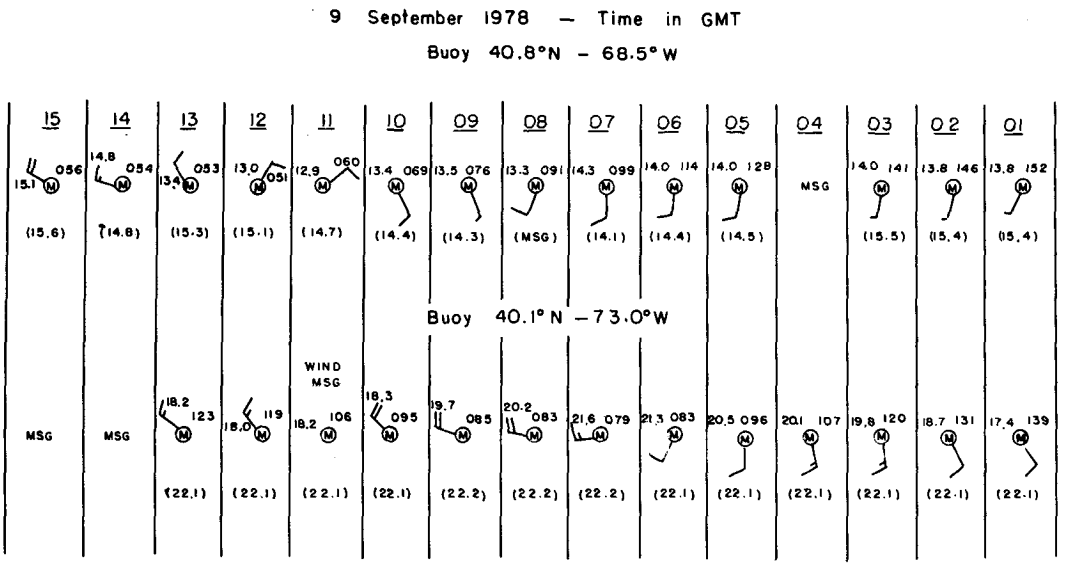

FIG. 7. Hourly time section of buoys located as shown, with plotting convention as in Fig. 3. Sea-surface temperatures are indicated in °C.

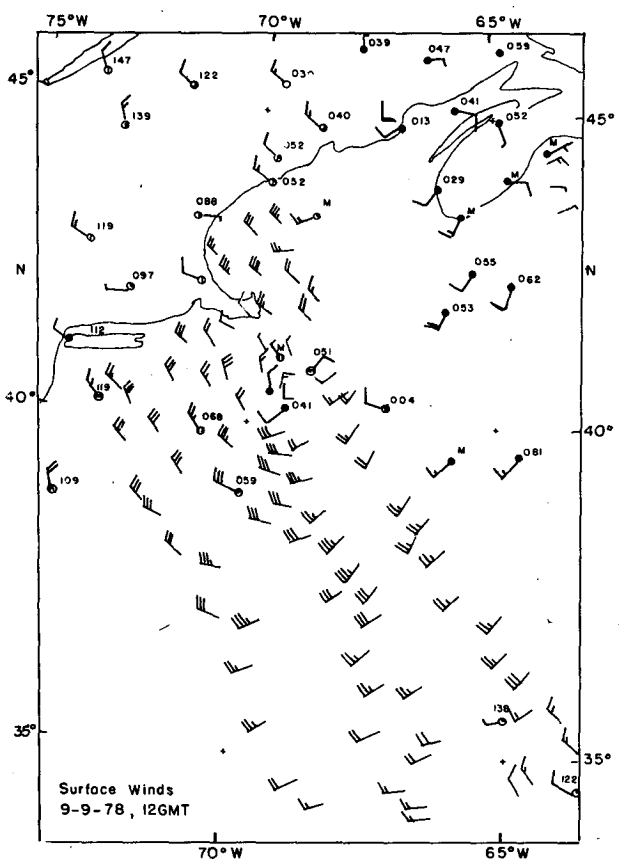

FIG. 8. Surface winds at 1200 GMT 9 September with Seasat, ship and land station winds included. Seasat observations are plotted without circles, while cloud amounts and sea-level pressures are plotted at the traditional reporting stations. Plotting convention as in Fig. 3.

FIG. 10 indicates the track of the low subsequent to 1200 GMT on the 9th, along with a composite SST analysis constructed using data for the preceding three-day period. Note the low center exists over a relatively uniform sea temperature of about 22°C until after 0000 GMT on the 10th. This fact, combined with the movement to the left of the upper tropospheric flow toward cooler mean tropospheric temperatures (see Fig. 9) implies a decrease of mean tropospheric static stability following the low center. The possibility for deep convection near the center thus increases with time. An elaboration of this point is presented in later sections. The strong low-level warm advection and its associated upward motion and pressure falls eastward of the low, clearly point to this shallow system moving to the left of the mean northwesterly tropospheric flow. This left movement of the surface low is opposite to what is usually observed in a typical, developing baroclinic wave (see Sanders, 1971; Austin, 1947). This same behavior was noted by Bosart (1981) for the incipient stages of the explosively-developing President's Day 1979 cyclone.

By 0000 GMT on the 10th, the low was east of the 1000–250 mb thermal trough (Fig. 11) and thus appeared to be in a more favorable position to intensify than was shown 12 h earlier as a result of the associated positive thermal vorticity advection (PTVA). At this time, a slight anticyclonic curvature in the thermal wind pattern directly over the surface low is shown. Unfortunately, there are no reporting ships near the center to confirm the conservative central pressure estimate of 990 mb.

There is little doubt, however, of the extraordinary intensity of the surface system at 1200 GMT on the

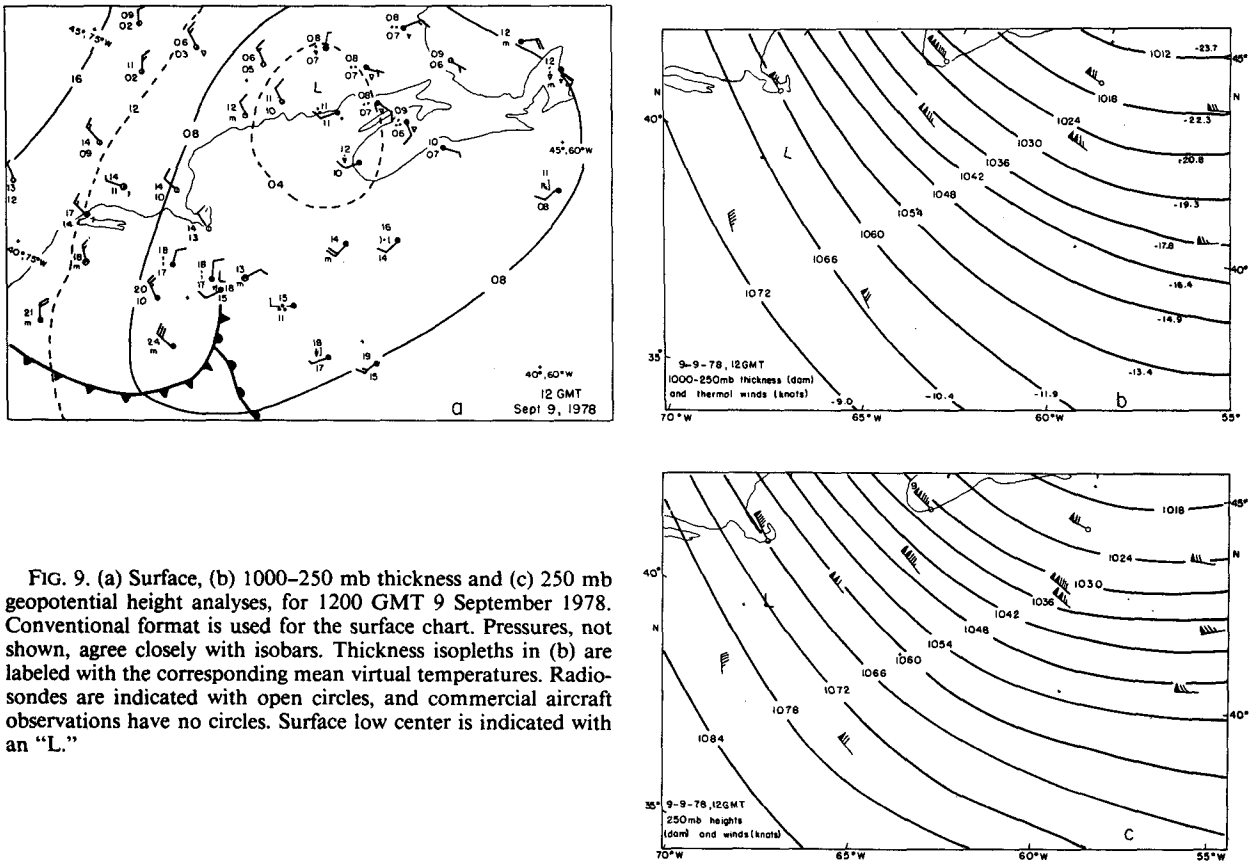

FIG. 9. (a) Surface, (b) 1000–250 mb thickness and (c) 250 mb geopotential height analyses, for 1200 GMT 9 September 1978. Conventional format is used for the surface chart. Pressures, not shown, agree closely with isobars. Thickness isopleths in (b) are labeled with the corresponding mean virtual temperatures. Radiosondes are indicated with open circles, and commercial aircraft observations have no circles. Surface low center is indicated with an "L."

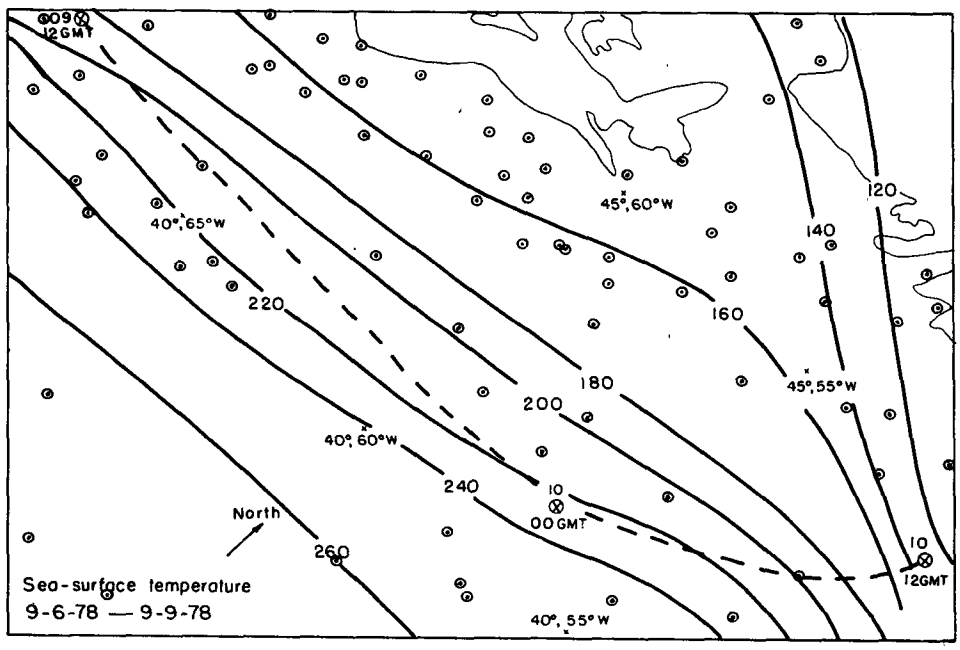

FIG. 10. Track of the surface cyclone along composite sea-surface temperature analysis based upon ship observations, the locations of which are indicated with dots, for the three-day period prior to 1200 GMT 9 September 1978. Temperatures are labeled in °C × 10.

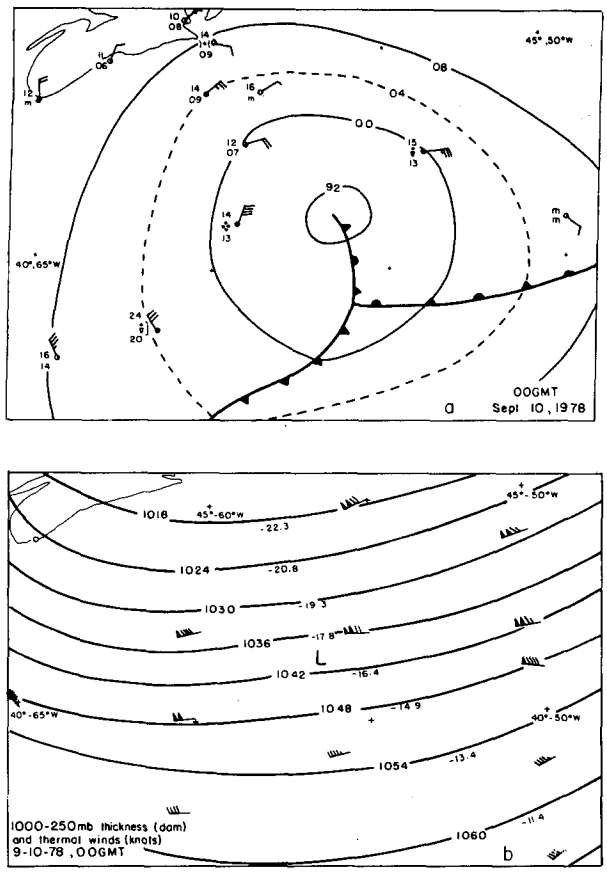

FIG. 11. (a) Surface and (b) 1000–250 thickness charts for 0000 GMT 10 September. Format as in Fig. 9.

10th. By this time, the central pressure had plunged to an estimated 945 mb. As is shown in Fig. 12, the *Euroliner* had passed very close to the cyclone center. Indeed, the *Euroliner* barogram (Fig. 1) confirms the incredibly tight pressure gradient surrounding the surface system. The 55 mb pressure fall it experienced during its 12 h odyssey into the vicinity of the eye is followed by an even more dramatic 3 h pressure rise of 31 mb. The anomalously warm 1000–250 mb thickness value of 10 780 m (Fig. 12b) above the surface is supported by three critical commercial aircraft observations (adjusted for time) of wind and temperature. The central thickness value was estimated from the 250 mb height analysis (10 370 m over the surface low) and the 945 mb sea-level pressure estimate. This strong warm core over the surface center resembles that of a tropical cyclone. Unfortunately, the NMC final analysis shown in Fig. 13 did not capture either the extreme intensity or the correct position of the cyclone, due to the missing *Euroliner* observation, in spite of its real-time availability on the Service C teletype.

Note the wind direction of the ship just to the north of the NMC-analyzed surface center in Fig. 13 was changed to 35° in Fig. 12a. The 350° wind direction was indicated in real-time on the Service C teletype and was probably a faulty transmission that appears credible in the absence of the *Euroliner* information

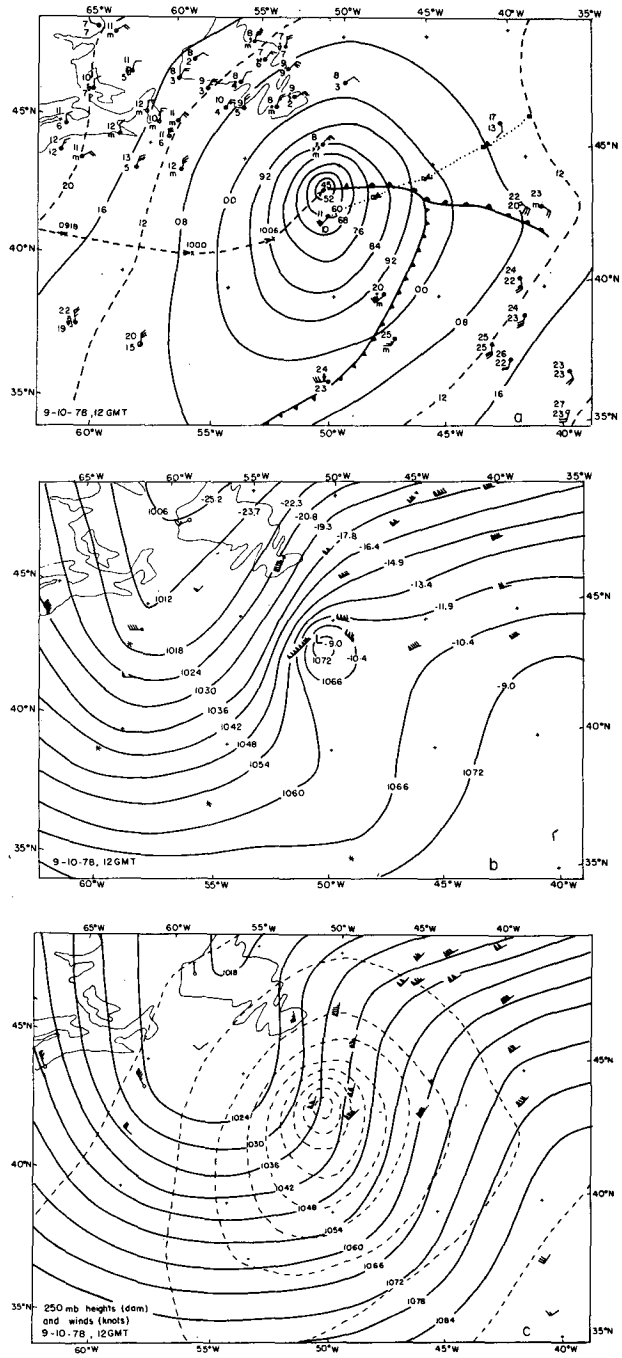

FIG. 12. As in Fig. 9, except for 1200 GMT 10 September 1978. (a) Surface chart indicates the paths and 6-hourly positions of the surface cyclone and of the *Euroliner*. (b) Thickness chart indicates locations (*'s) of satellite-derived thickness observations. (c) The 250 mb chart also shows sea-level isobars (dashed lines) illustrating how the thermal winds are computed.

and satellite imagery. The revised estimate of the correct position of the surface cyclone at this time is also confirmed by the GOES-east satellite image (not shown) and by the wind reports from orbit 1080 of Seasat. This plot of surface winds is shown in Fig. 14. Note the Seasat wind directions confirm the credibility of the aforementioned 35° wind direction. Although up to four possible directions are given for each Seasat point, the directions shown represent, in the author's view, the most consistent wind pattern. In fact, this subjectively de-aliased wind field is quite similar to Hoffman's (1982) objective representation of the winds, with the 35° wind direction introduced into his scheme (see his Fig. 7). With the originally-reported 350° wind direction, he retrieved a de-aliased Seasat wind field that was inconsistent with the synoptic circumstances of this case (his Fig. 4).

The observed (predominately Seasat) winds reinforce the *Euroliner* 1200 GMT pressure and wind report, and show the existence of hurricane force winds 110–170 km south and west of the surface center, while the resolution of these winds is sufficient to capture the minimum speeds of 10 m s^{-1} close to the surface center. Our extrapolation of the horizontal pressure gradient yields a central pressure of 945 mb. An overly conservative estimate of the central pressure based on inviscid, cyclostrophic flow, the *Euroliner* report, and on the Seasat winds, yields a central pressure of 947 mb.

We have noted the cyclone's warm core structure, and its hurricane force winds. We will now compare other characteristics with the tropical cyclone. Although the 110–170 km radius of maximum wind (RMW) is generally higher than the 65 km RMW usually found for a tropical cyclone (Gray and Shea, 1973), this distinction is a fine one; for RMW's in hurricanes are highly variable and occasionally do range much higher than the mean. The surface relative vorticity approached 50×10^{-5} s^{-1}, and is comparable to corresponding values found by Gray and Shea in the vicinity of the hurricane's eyewall region. Clearly, the profiles of wind and pressure bear a close resemblance to that of a tropical cyclone.

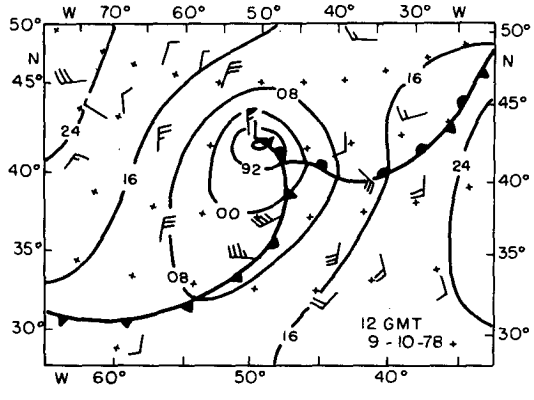

FIG. 13. NMC final surface analysis for 1200 GMT 10 September 1978. Winds only are plotted.

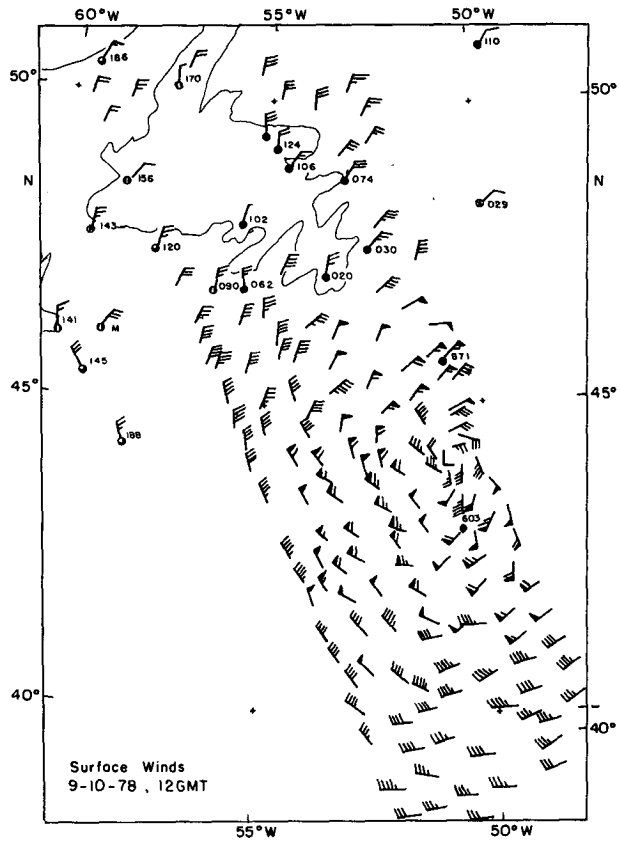

FIG. 14. Surface winds for 1200 GMT 10 September 1978 including land, ship, and Seasat reports. Format as in Fig. 8.

Satellite images covering the 25.5 h period prior to 1330 GMT on the 10th are shown in Fig. 15. Cyclone center positions were determined from the author's surface analyses; and for off-synoptic times, spatial and temporal interpolation was used between these 6 h positions. The 1200 GMT 9 September M_B-enhanced image shows the northern edge of the large MCC to be 280 km south of the developing surface center (southeast of Cape Cod) whose cloud tops are no higher than 800 mb. Clouds over the surface cyclone continue to deepen until at 1700 GMT with the MCC and the surface low diverging, a small area of deep clouds over the surface cyclone extends above 350 mb (not shown). The area covered by deep convective cells continues to expand and the cloud tops rise during the next 12 h. The DMSP infrared image at 0350 GMT on the 10th shows the extreme intensity of the storm (centered at 41.9°N, 55.1°W), with the deepest convective cells as close as 100 km northeast of the center. Evidence for the strong surface circulation is seen in the form of open convection cells to the center's southwest and the associated cold air pen-

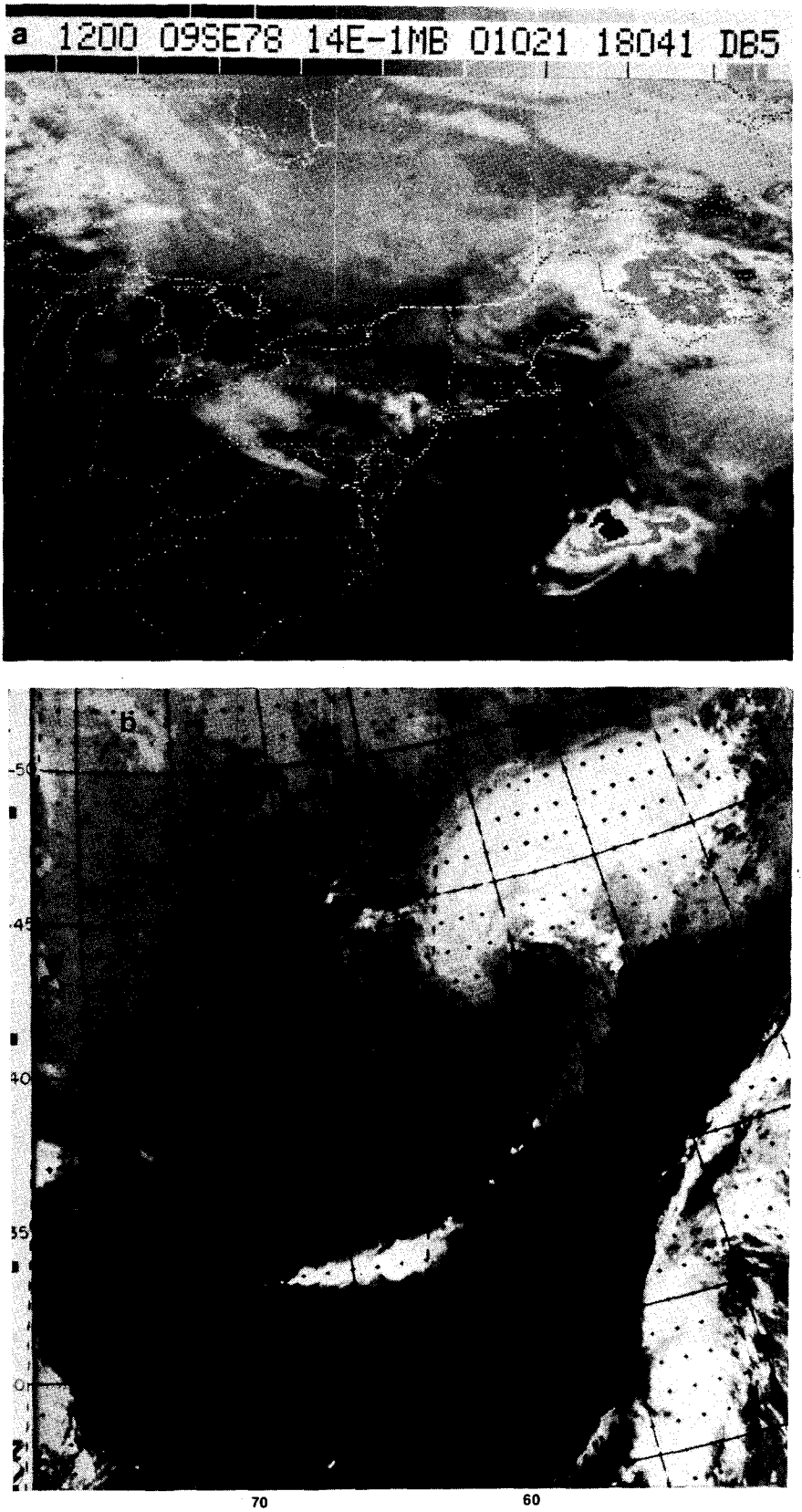

FIG. 15. (a) As in Fig. 5, except for 1200 GMT 9 September 1978. (Misgridding: shift gridding northward ~30 km relative to image.) (b) DMSP infrared image for 0350 GMT 10 September 1978. Gridding is accurate. (c) As for (b) except for 0859 GMT 10 September 1978. (d) As for (b) except for the DMSP visible image for 1330 GMT 10 September 1978. Circles denote surface cyclone location in each part, except (d) in which the cloud free area at 44°N, 49.8°W shows the center.

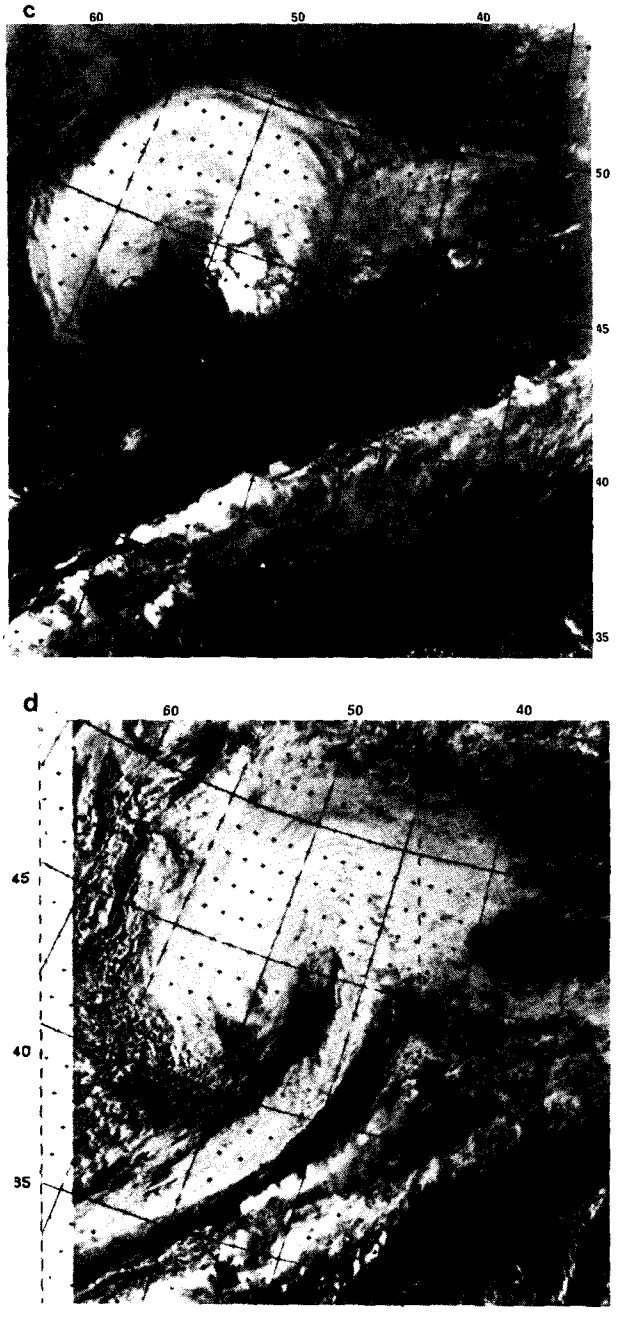

FIG. 15. (*Continued*)

etrating southward to 33°N. By 0900 GMT on the 10th, the area of deepest convection has moved off to ~300 km northeast of the storm center (41.7°N, 52.9°W), which is essentially cloud-free. It is hypothesized that the surface low has reached peak intensity by this time due to the deepest cloud moving away from the storm center, and its movement over cooler waters (Fig. 10) at this time. This implies the storm intensified even more rapidly than the rate indicated in the previous map discussion, and the low could have reached a central pressure considerably lower than our 1200 GMT 945 mb estimate. The visible image for 1330 GMT shows a cloud-free eye-like storm center, though the infrared image (not shown) for the same time shows the nearby clouds to be relatively shallow and the deep convection well off to the east and northeast to be lined up along the frontal band shown in Fig. 12.

When compared with Holliday and Thompson's (1979) sample of 305 typhoons at mean latitude 18°N, the extremely rapid development of this surface cyclone at 59 mb in 24 h at 42°N would represent a geostrophically equivalent 24 h pressure fall of greater than 27 mb. This would place the *QE II* case at the 57th percentile of their sample of 24 h typhoon deepening rates. The deep convection associated with the cyclogenesis along with the hurricane force winds, the clear eye-like center and the intense tropospheric warm core are all similarities to that of a tropical cyclone in this otherwise extratropical case.

4. Operational model performance

The NMC LFM-II initial analysis for 1200 GMT on the 9th, along with the resulting 12 h and 24 h forecasts are shown in Fig. 16. The model does proceed with cyclogenesis in approximately the correct locations. The major problem is with the intensity forecast. The central pressure forecast of 1000 mb for 1200 GMT on the 10th is 55 mb higher than what was actually observed. The corresponding wind and wave forecasts for the affected area were thus egregiously erroneous. As an example, the forecast maximum geostrophic wind just to the north of the center was ~15 m s^{-1}, while Fig. 12 shows geostrophic wind speeds to the north and west of the center to be 150 m s^{-1}. The problem was exacerbated by the fact that even the real-time analysis of the situation at 1200 GMT on the 10th (see Fig. 13) grossly underestimated the severity of this storm. The LFM-II product is the result of a numerical integration of the primitive equations (see Shuman and Hovermale, 1968; and Gerrity, 1977), and its horizontal grid mesh length is approximately 120 km. For such a large system with observed winds of at least 15 m s^{-1} extending at least 1100 km from the storm center in all directions (see Fig. 14), the 120 km grid spacing does not appear to be the primary source of the problem.

The operational FNWC product is shown for the same three times in Fig. 17. The intensity forecast is similarly deficient to that of the LFM-II with the 999 mb center being forecast for 1200 GMT on the 10th. The slow displacement of the surface system is one additional problem the LFM-II did not have and may be attributed to the FNWC model's coarse horizontal resolution of about 381 km. This primitive equation model is discussed in Kesel and Winninghoff (1972).

The problem of underforecasting maritime cyclogenesis is well-known, and has been documented by Leary (1971), SG, and more recently by Silberberg and Bosart (1982). Since this deficiency has been relatively insensitive to the increase in the horizontal

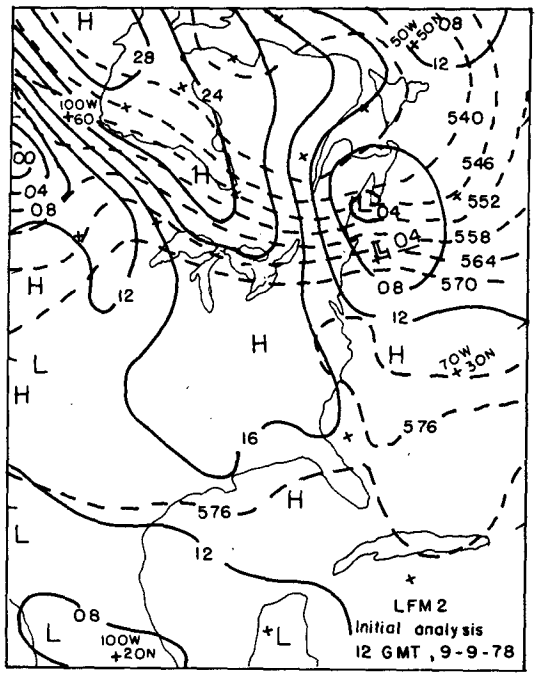

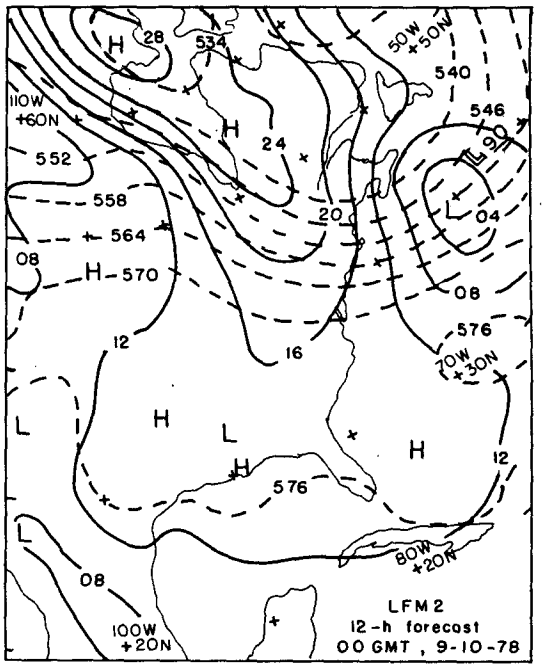

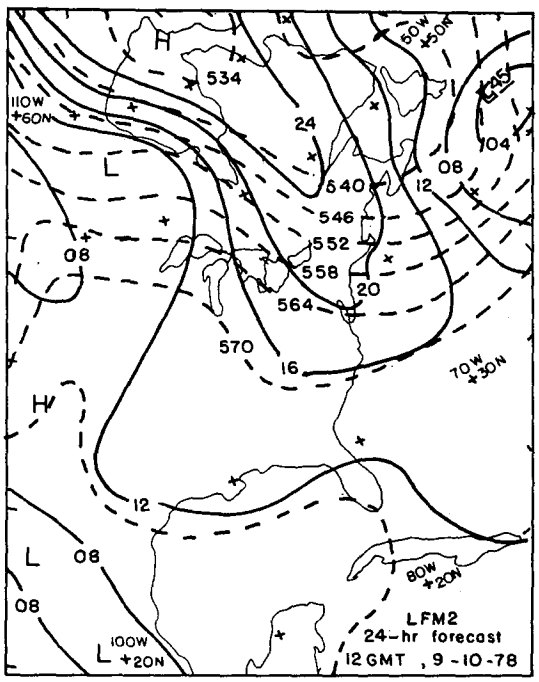

FIG. 16. LFM-II initial analysis, 12 h and 24 h forecasts, for the 24 h period beginning 1200 GMT 9 September 1978, of sea level pressure, and 1000–500 mb thickness. Sea level pressures (mb, hundreds and thousands digits omitted) are analyzed in solid lines, and thicknesses are in dashed lines. Observed position (indicated by a double L) and central pressure of surface low are also shown in each panel.

grid resolution, the trend to faster computing machines and therefore to finer mesh models does not represent the sole solution to this problem.

In order to explore possible reasons for the numerical model's poor performance, the role that adiabatic, inviscid quasi-geostrophic dynamics may have played in this storm's evolution is examined in the next section. A careful compilation of all existing data for this case will be utilized in order to examine this role as accurately as possible.

5. Vertical motions and quasi-geostrophic diagnosis

Kinematically-computed vertical motion profiles for the Wallops–Fort Totten–Dulles triangle for 0000 GMT 9 September are shown in Fig. 18. These profiles were computed from wind data at approximately 30 mb intervals from 1000 to 100 mb. Omega is assumed zero at the lower boundary with a constant correction applied to the divergence profile so that omega is zero at 100 mb. The low at this time is

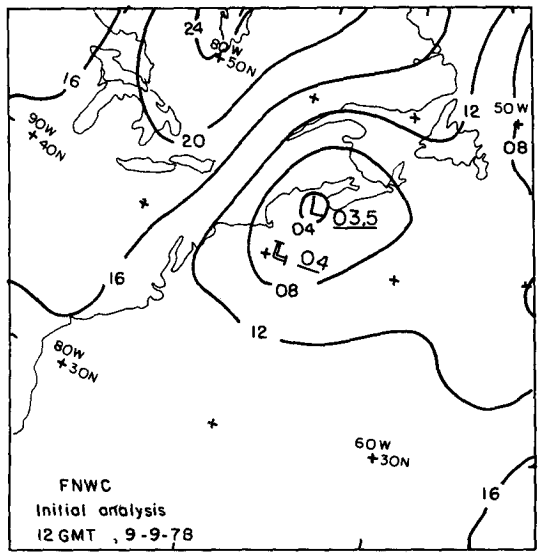

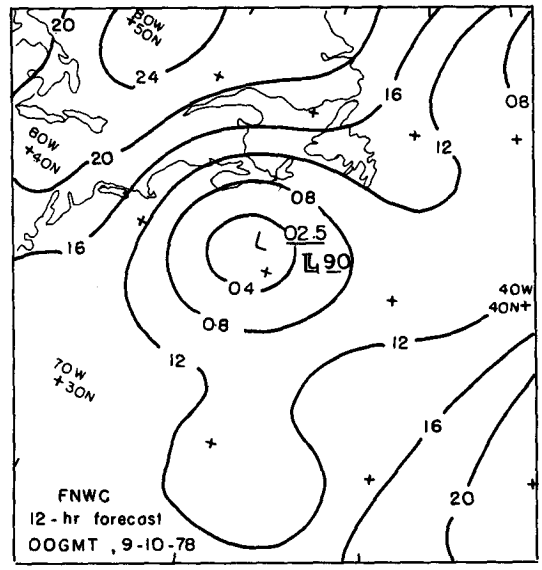

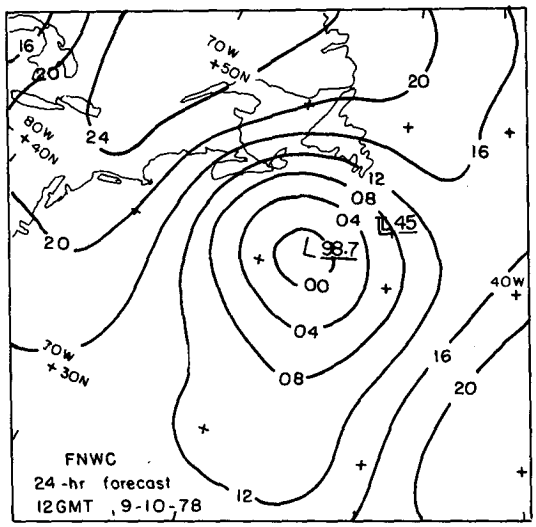

FIG. 17. As in Fig. 16 except for the FNWC-PE model output with thicknesses not included.

located approximately at the centroid of this triangle (Fig. 3). The slight upward motion, peaking below 940 mb in the uncorrected profile, indicates the triangle-scale upward motion is quite shallow, as is the surface low. Strong triangle-scale subsidence is shown in the middle and upper troposphere.

Vertical motion profiles have also been computed in the vicinity of the surface cyclone for 1200 GMT on 9 and 10 September. These profiles are based upon independent wind analyses at the surface and 250 mb from which the divergence calculations described earlier were performed. The divergence profiles, constructed for each grid point, are assumed linear from 1000 to 100 mb with observed surface and 250 mb values specifying these lines. The resulting kinematically-computed profile for grid point 40°N, 68°W is shown in Fig. 19. The corrected profile is found in the manner discussed earlier. The agreement in sign of the corrected and uncorrected ω's is encouraging. However, our procedure also specifies the level of maximum vertical motion to be 550 mb—likely to be unrealistic for this time when the disturbance is still confined to the lower troposphere. In spite of this caveat, the horizontal distribution of ω at 550 mb, shown in Fig. 19, agrees qualitatively with the known locations of the low and of the MCC.

By 1200 GMT on the 10th, with the low at or near peak intensity, the strong outflow at 250 mb over the surface cyclone, and northeastward to the deep cumulonimbus cells, is shown in the 250 mb wind observations and in the resulting divergence field (Fig. 20). The surface divergence pattern, also shown in Fig. 20, is generally consistent with the 250 mb divergences. The resulting vertical motions in and around the surface low have more than tripled in 24 h, with corrected ω's on the order of -50×10^{-3} mb s^{-1} at four grid points near the center, though the likely breakdown of the linear divergence assumption

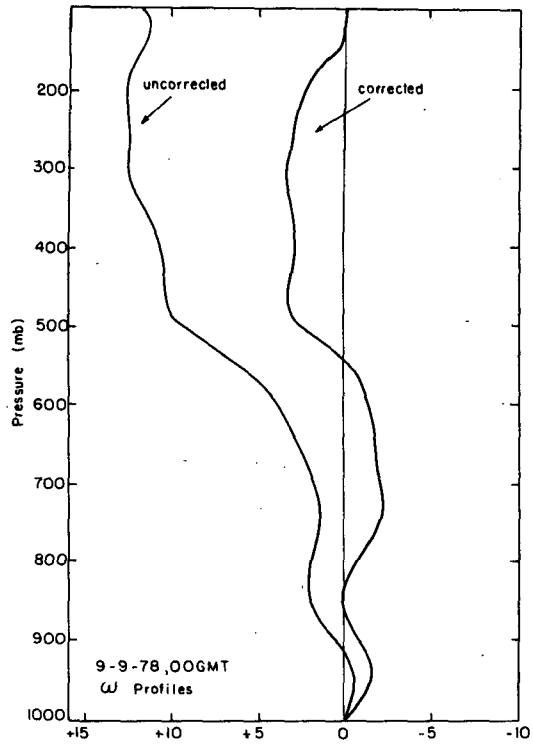

FIG. 18. Profiles of kinematically computed omega (units of 10^{-3} mb s^{-1}) for the triangle defined by Wallops Island, Virginia (WAL), Fort Totten, New York (JFK), and Dulles International Airport (IAD).

causes us to question the level at which the ascent maxima are located. These vertical motions are quite close to the -58×10^{-3} mb s^{-1} mean value found in the eyewall region of tropical cyclones (see Gray and Shea, 1973).

To gain a quantitative understanding of the quasi-geostrophic forcing taking place during the cyclone development, the thickness field at 0000 GMT 10 September has been used to diagnose the instantaneous central pressure tendency. This tendency is computed from the geopotential fall found in the quasi-geostrophic model discussed in SG (a modification of the Sanders (1971) analytical model). Table 1 shows the values of the various parameters used in the computation, each of which is defined in the Appendix. The active deepening mechanism in the model is the cyclonic thermal vorticity advection over the surface cyclone center. The dimensionless static stability parameter $\gamma = 0.063$ represents the mean thermal stratification (referred to the moist adiabat) found in the 68 weather ship radiosonde observations described in SG. The computed instantaneous 12 h central pressure fall of 3.6 mb falls far short of that which is observed. From our knowledge of the storm's evolution, a conservative estimate of the instantaneous deepening rate at this time is 29 mb. The computations were made assuming λ to be $L/4$, the atmosphere to be saturated (thus minimizing the effective static stability), and the frictional filling effect

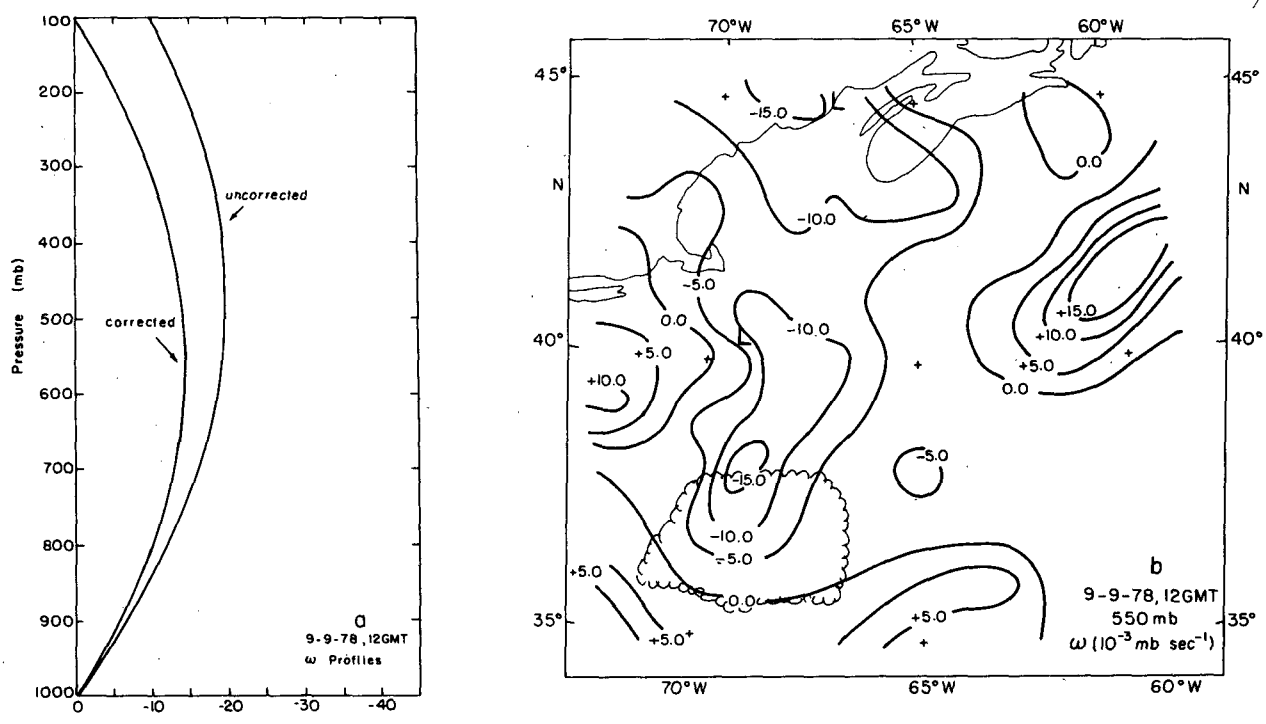

FIG. 19. (a) Vertical motion profile close to the surface cyclone center (40°N, 68°W) for 1200 GMT 9 September and (b) corrected ω's for 550 mb. Units are 10^{-3} mb s^{-1}. L's indicate the surface cyclone positions. The curled area outlines the area enclosed by the MCC.

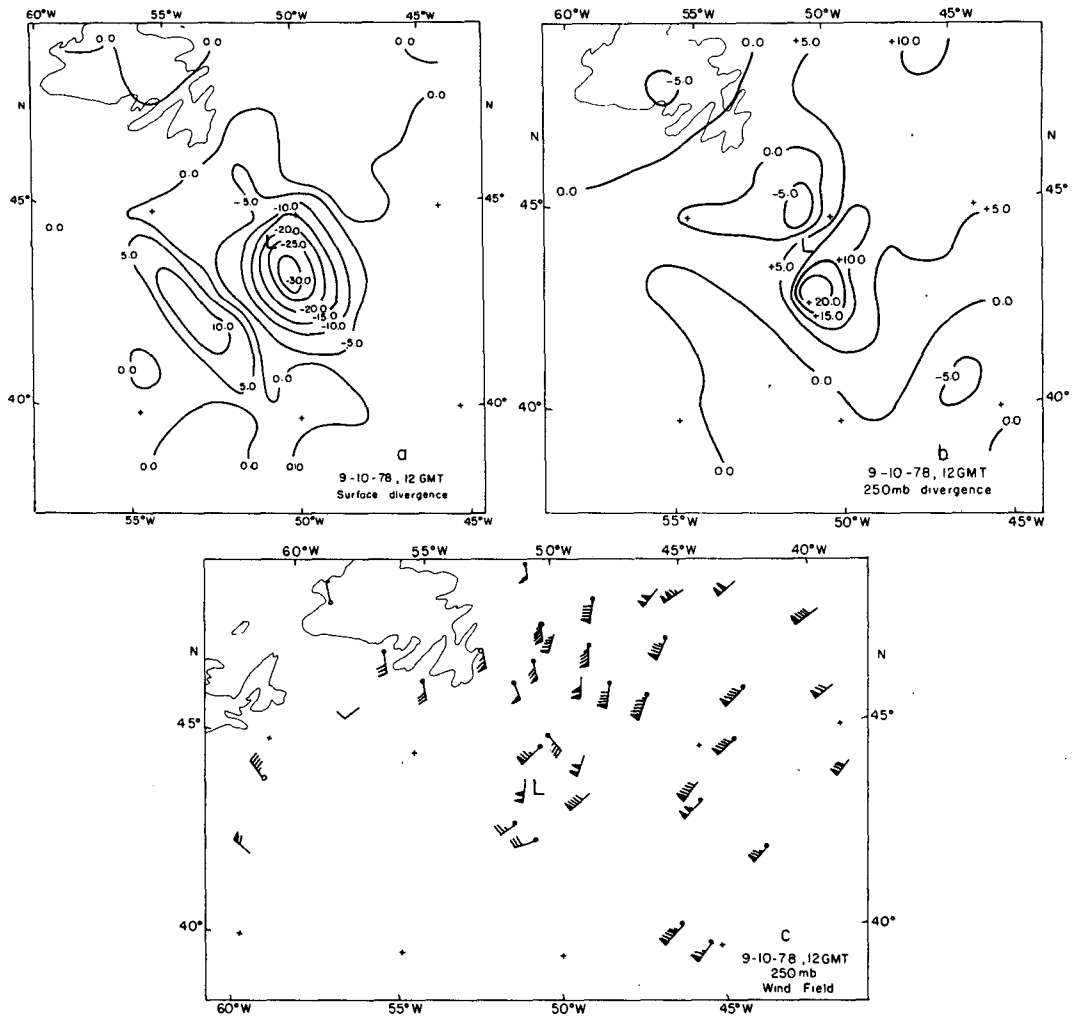

FIG. 20. (a) Surface and (b) 250 mb horizontal divergence (units of 10^{-5} s^{-1}) for 1200 GMT 10 September. (c) The 250 mb wind field on which the divergence calculations are based is also shown. Closed circles indicate satellite-derived winds.

TABLE 1. Quasi-geostrophic parameters used in the model to compute the cyclone's central pressure tendency at 0000 GMT 10 September 1978 [see Sanders and Gyakum (1980) for further details].*

Parameter	Model value
L	1800 km
a	1.16×10^{-5} K m^{-1}
$\hat{T}$	1.0 K
f_0	0.99×10^{-4} s^{-1}
η_0	1.8×10^{-4} s^{-1}
T_0	250 K
γ	0.063
λ/L	0.19
χ_{10}	−3.3 mb/12 h (without λ correction) −3.6 mb/12 h

* Observed instantaneous central pressure tendency at 0000 GMT 10 September was −29 mb/12 h.

has been ignored. Thus, the maximum amount of intensification has been extracted from this quasi-geostrophic model, for the above-mentioned physical effects would each tend to reduce our computed central pressure fall.

As an additional check on quasi-geostrophic forcing taking place within this system, we have utilized a more complicated version of the previous model. The model differs from the previous one discussed in that the thermodynamic structure is specified in three distinct layers. The lowest layer has the maximum horizontal temperature contrast. The depth of each layer is determined by the synoptic analysis for each computation. The goal is to allow for vertical differences in the horizontal temperature contrast. Thus, we may focus upon the strong low-level vertical wind shear observed in this case. Further details of the model are given in the Appendix. Indeed, we have

seen this disturbance to be quite shallow through 1200 GMT on the 9th, and a much stronger baroclinic zone exists in the lower troposphere than in the upper levels (Figs. 3, 6 and 10). More generally, SG has shown the low-level baroclinicity as being particularly strong in the vicinity of oceanic "bomb" frequency maxima. Staley and Gall (1977) have used a four-level quasi-geostrophic model to show the importance of both low static stability and strong wind shear in the lower layers in the enhancement of short baroclinic wave growth. More recent theoretical work by Satyamurty *et al.* (1982) has shown small scale (~1000 km) baroclinic waves to have their amplitude confined to the lower troposphere.

The expression for the geopotential tendency is given in the Appendix. We used the 1000–850 mb thickness field (derived in precisely the same manner as for the 1000–250 mb thickness fields and shown in Fig. 21a) to compute the low-level temperature structure. The winds used were 850 mb radiosonde winds and low-level cloud winds derived from the GOES-east imagery. Table 2 presents the results of our computations. The instantaneous deepening rate of 3.2 mb/12 h still falls far short of the observed estimate of 11 mb 12 h, but is an improvement over the zero deepening we would have computed had we used the total tropospheric thermal field for this time (Fig. 9), as is required by the cruder quasi-geostrophic model discussed in SG.

For these computations, γ is based on the observed stratification with respect to the moist adiabat, λ is assumed to be $L/4$, and frictional filling has been ignored. Even a halving of the low-level static stability (the one parameter about which we are most uncertain) will raise the central pressure fall to only 4.7 mb/12 h. As a more graphic illustration of the problem, the quasi-geostrophic vertical motion profiles over the center, on which these calculations are based, are shown in Fig. 21b. The vertical motion ω_{11} is forced by positive thermal vorticity advection, while ω_{12} is forced by the advection of earth vorticity by the thermal wind. This latter component is negligibly positive and, therefore, represents a slight brake on the cyclone's quasi-geostrophic intensification. A comparison with Fig. 19 shows this quasi-geostrophic estimate to be only a third of what the probable maximum ascent actually was over the center.

Further computations using this model in a relatively data-rich area, have been performed with the most optimal pattern of surface isotherms, found at 0300 GMT 9 September (similar to those found in Fig. 3). The resulting computed fall of 2.7 mb/12 h still falls short of the observed fall of 7 mb/12 h.

We conclude from all of this that shallow baroclinic forcing initiated the cyclonic surface development at 0000 GMT 9 September, but its accelerated development by 0300 GMT on the 9th, and indeed throughout its life cycle, cannot be accounted for by

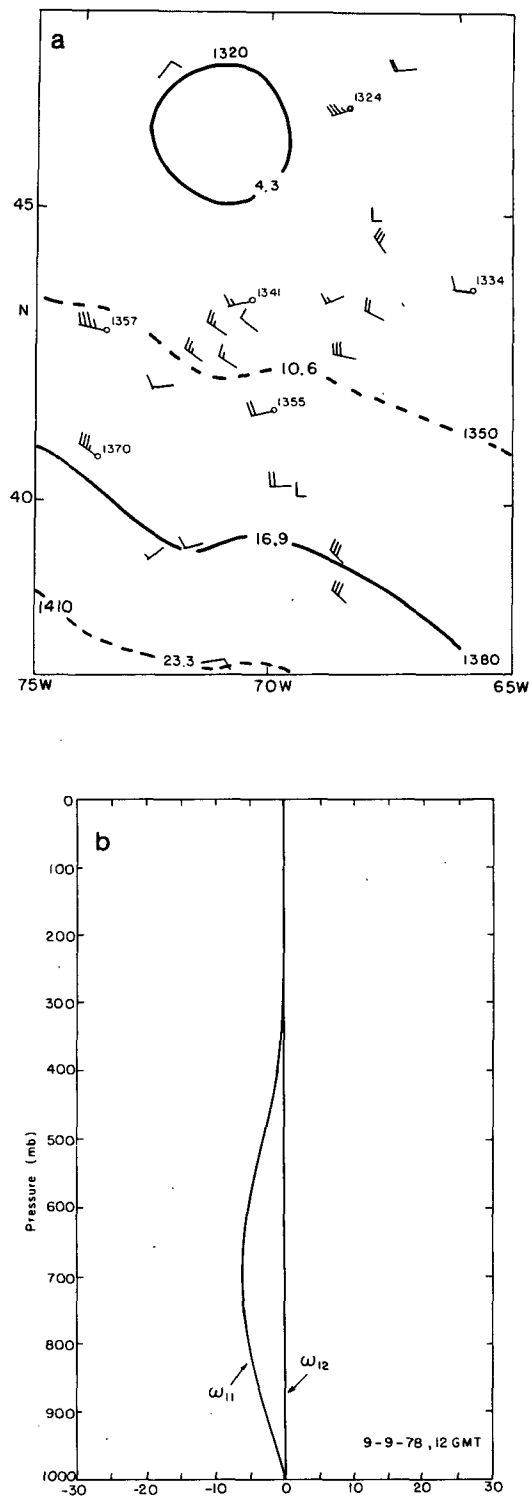

FIG. 21. (a) 1000–850 mb thickness analysis for 1200 GMT 9 September with isopleths also labeled with the corresponding mean virtual temperatures (°C). The surface low center is indicated with an "L." Radiosondes are indicated with open circles, and satellite wind observation points have no circles. Units are in m. (b) Quasi-geostrophic profiles of ω_{11} and ω_{12} at $\lambda = L/4$. Units are 10^{-3} mb s^{-1}.

TABLE 2. Quasi-geostrophic parameters used to compute central pressure tendency at 1200 GMT 9 September 1978 (see Appendix for further details).*

Parameter	Value
P_2	800 mb
P_3	400 mb
L	1100 km
a	2.50×10^{-5} K m^{-1}
$\hat{T}$	0.9 K
f_0	0.94×10^{-4} s^{-1}
η_0	1.3×10^{-4} s^{-1}
T_0	250 K
γ	0.058
λ/L	0.30
χ_{10}	−3.2 mb/12 h (without λ correction)

* Observed instantaneous central pressure tendency at 1200 GMT 9 September was −11 mb 12 h^{-1}.

adiabatic (excluding the effect of latent heat release in saturated cyclone-scale ascent), inviscid quasi-geostrophic dynamics. The fact the operational numerical models also produced a comparably poor simulation of the observed explosive cyclogenesis indicates that incorporation of the model's assumed superior physics (including non quasi-geostrophic effects) was not helpful in producing a successful simulation. Although data-deficient initial fields may have contributed to the poor forecasts, other physical processes may be responsible for the observed rapid development. The observed deep convection in and around the developing storm center is a plausible process through its dynamic and thermodynamic effects on the cyclone scale. These effects have not been incorporated into our models and may be improperly simulated in the operational models, as has been suggested by Tracton (1973).

6. Summary and Discussion

The powerful cyclone which battered the liner *Queen Elizabeth II,* and in which the dragger, *Captain Cosmo,* was lost originated as a shallow baroclinic disturbance over the middle Atlantic states. This disturbance appears to have developed just after 0000 GMT 9 September as a result of a favorable low-level thermal trough–ridge pattern due to rain-cooled surface air existing westward of a warmer maritime environment (Fig. 3). The low was "steered" by the low-level warm advection, associated with intense sea-surface temperature contrasts, to the left of the upper-level flow in contrast to the instantaneous motions of most lows. This early development and steering, dictated by the existing mesoscale environment, appears responsible for the surface cyclone environment becoming hydrostatically and dynamically less stable through increasingly deep layers with time. Thus, the mesoscale conditions in the storm's incipient stages are linked with the storm's subsequent explosive development on the synoptic scale.

The early development also took place in the clear air just to the northwest of a rapidly developing MCC. Many tropical cyclones also initially develop under similar circumstances, as has been shown observationally by Weickmann *et al.* (1977), and by Fingerhut and Gray in Grube's (1979) work. Although we have described conditions which point to some of the early rapid cyclogenetic development to have been associated with the developing MCC (prior to 0600 GMT 9 September), the MCC appears to have been unrelated to the explosive cyclogenesis documented subsequent to 1200 GMT 9 September. The deep convection which seems important for the explosive development first appeared at 1700 GMT 9 September when the MCC was 450 km southwest of the cyclone center. The subsequent vertical and horizontal growth of this convection area was concurrent with the cyclone's most explosive development.

The storm deepened nearly 60 mb in the 24 h period subsequent to 1200 GMT 9 September in association with an initially shallow lower tropospheric short-wave trough and with deep cumulus convection in and around the storm center. The rapidity with which this storm intensified and grew in size to supersynoptic scale by 11 September (James, 1979) makes such a class of cyclone even more dangerous to marine interests than are tropical cyclones. Operational numerical models missed virtually all of the cyclone intensification, and the NMC final surface analysis at 1200 GMT on 10 September overestimated the storm central pressure by 35 mb owing to the absence of the *Euroliner* observation. This datum existed on the Service C network and, along with the *Euroliner* weather log and barograph trace, proved to be crucial in more correctly estimating the storm's central intensity. This fact should serve as a caveat to those whose sole contact with the current weather is based upon the use of final NMC-analyzed meteorological fields.

The Seasat-A surface wind fields also proved to be instrumental in capturing the cyclone's central intensity and reinforced the *Euroliner* observations. The hurricane force winds shown by the Seasat instrumentation package represent important information to the meteorologist and to the mariner had they been available in real-time. This type of instrumentation package would be a major boon to the present surface maritime observing system.

We have shown the surface winds to be of hurricane force, storm-scale surface relative vorticities and ascent to be comparable to those found in tropical cyclones, and the rapid 24 h central pressure fall to be greater than those found in the majority of typhoons. The deep convection in and around the storm center, the clear eyelike center at the storm's mature stage, and the intense tropospheric warm core

are all features found in tropical cyclones. What distinguishes this cyclone from tropical cyclones includes its strong low-level baroclinic zone and asymmetric distribution of convection with respect to the center. The development of the upper-level trough occurred after the surface low appeared, in a manner similar to that discussed by Bosart (1981) for the President's Day snowstorm.

Quasi-geostrophic computations of vertical motions and central pressure tendencies performed throughout the life cycle of this cyclone reveal solutions which fall far short of the "observed" vertical motions and intensification. However, the use of a three-layer quasi-geostrophic model did allow us to compute some deepening using a lower tropospheric thickness pattern at 1200 GMT 9 September, while the use of the tropospheric thickness field in a similar analysis yields zero deepening. At this time, the model does show upward motion sufficient to lift the potentially unstable air and set off the convection in and around the storm center a few hours later. Thus, while the quasi-geostrophic ascent was insufficient alone to account for the observed instantaneous intensification, this effect may have been critical for the cyclone evolution, through its triggering and organization of the convection. Suggestions have already been made in the literature that convection may be of critical importance in extratropical cyclogenesis (see, for example, Tracton, 1973; Rasmussen, 1979; Reed, 1979; and Bosart, 1981). Part II of this study will explore the probable role that cumulus convection played in the explosive cyclogenesis found in the *QEII* case.

APPENDIX

Further Details of the Model

The three-layer quasi-geostrophic model differs from that described in SG in that the horizontal temperature gradient is assumed independent of height from 1000 mb (P_0) only up to some specified pressure level P_2. A linear decrease with pressure of this temperature gradient takes place from P_2 up to another specified pressure height P_3, where it is assumed zero. Above this level, the horizontal temperature gradient is assumed zero to the top of the atmosphere. The expression used for the geopotential tendency at the surface low center χ_{10}, is

$$\chi_{10} = \hat{\chi}_{10} \sin(2\pi\lambda/L), \tag{1}$$

where L indicates the wavelength of the synoptic-scale thermal trough-ridge pattern, and λ is the upstream displacement of the surface center from the warm ridge. Therefore, $\hat{\chi}_{10}$ is the height tendency of the low center located a distance $L/4$ upstream from the warm ridge. In this model

$$\hat{\chi}_{10} = \frac{f_0\eta_0}{-b_1}\left[\frac{q_1(A+A_4)}{P_3}\left(\frac{P_3}{P_0}\right)^{q_1} - \frac{(C+C_4)}{P_2}q_1\left(\frac{P_2}{P_0}\right)^{q_1} + \frac{(E+E_4)q_1}{P_0} + (D+D_4)\left(\frac{P_2}{P_0}\right)^{q_1} - (B+B_4)\left(\frac{P_3}{P_0}\right)^{q_1} + \frac{a_1k_1}{b_1^2} + \frac{(k_1-k_4)}{b_1}\right], \tag{2}$$

where the variables are as follows:

$$k_1 = \left(\frac{2\pi}{L}\right)^3 \frac{Ra\hat{T}}{T_0\gamma}\left(\frac{4}{f_0}\right),$$

$$k_4 = \left(-\frac{2\pi}{L}\right)\frac{\hat{T}}{\gamma T_0}\left(\frac{\partial f}{\partial y}\right)_0,$$

$$A = \left(\frac{-M_2P_3^3}{(6a_1-b_1)}\right) - \frac{3a_1M_2P_3^3}{(2a_1-b_1)^2} + \frac{2a_1P_3^2\left[M_1 + M_2P_2 + M_2P_3\ln\left(\frac{P_3}{P_2}\right)\right]}{b_1(2a_1-b_1)} + \frac{M_2P_3^3}{(2a_1-b_1)} + \frac{a_1M_2P_3^3}{b_1^2},$$

$$B = \frac{-3M_2P_3^2}{(6a_1-b_1)} - \frac{6a_1M_2P_3^2}{(2a_1-b_1)^2} + \frac{(2a_1+b_1)M_1P_3}{(2a_1-b_1)b_1} + \frac{2(a_1+b_1)M_2P_3^2}{(2a_1-b_1)b_1} + \frac{(2a_1+b_1)M_2P_2P_3}{(2a_1-b_1)b_1} + \frac{a_1P_3^2M_2}{b_1^2} + \frac{(2a_1+b_1)M_2P_3^2\ln\left(\frac{P_3}{P_2}\right)}{(2a_1-b_1)b_1},$$

$$C = \frac{a_1P_2(P_3^2M_2-k_1)}{b_1^2} + \frac{P_2\left[M_1P_3 - k_1\ln\left(\frac{P_2}{P_0}\right)\right]}{b_1} - \frac{M_2P_2^3}{(6a_1-b_1)} - \frac{3a_1M_2P_3P_2^2}{(2a_1-b_1)^2} + \frac{P_2^2(M_1+P_2M_2)}{(2a_1-b_1)} + \frac{2a_1M_2P_3P_2^2}{b_1(2a_1-b_1)},$$

$$D = \frac{a_1(P_3^2M_2-k_1)}{b_1^2} + \frac{P_3(M_1+P_3M_2)}{b_1} - \frac{k_1}{b_1}\left[\ln\left(\frac{P_2}{P_0}\right)+1\right] - \frac{3M_2P_2^2}{(6a_1-b_1)} - \frac{6a_1M_2P_3P_2}{(2a_1-b_1)^2} + \frac{2P_2(M_1+M_2P_2)}{(2a_1-b_1)} + \frac{2(a_1+b_1)M_2P_2P_3}{b_1(2a_1-b_1)},$$

$$E = \frac{-a_1 P_0 k_1}{b_1^2},$$

$$A_4 = \frac{2a_1 M_4 P_3^2}{b_1(2a_1 - b_1)},$$

$$B_4 = \frac{(2a_1 + b_1)M_4 P_3}{b_1(2a_1 - b_1)},$$

$$C_4 = \left[\frac{M_4 P_2^2}{(2a_1 - b_1)} + \frac{P_2(P_3 M_4 + k_4)}{b_1}\right],$$

$$D_4 = \frac{2M_4 P_2}{(2a_1 - b_1)} + \frac{(M_4 P_3 + k_4)}{b_1},$$

$$E_4 = \frac{k_4 P_0}{b_1},$$

$$M_1 = \frac{4Ra\hat{T}}{f_0(P_2 - P_3)T_0\gamma}\left(\frac{2\pi}{L}\right)^3 \ln\left(\frac{P_0}{P_2}\right),$$

$$M_2 = \frac{4Ra\hat{T}}{f_0(P_2 - P_3)^2\gamma T_0}\left(\frac{2\pi}{L}\right)^3,$$

$$M_4 = \frac{-\hat{T}}{\gamma T_0(P_2 - P_3)}\left(\frac{2\pi}{L}\right)\left(\frac{\partial f}{\partial y}\right)_0,$$

$$a_1 = \frac{f_0\eta_0}{RT_0\gamma},$$

$$b_1 = 2\left(\frac{2\pi}{L}\right)^2,$$

$$q_1 = \tfrac{1}{2} + \tfrac{1}{2}[1 + 4(b_1/a_1)]^{1/2}.$$

The term a is a measure of the mean planetary-scale temperature gradient, while $\hat{T}$ is the perturbed part of the temperature field. Other symbols include R (the gas constant), T_0 (the mean tropospheric temperature), η_0 (the domain-averaged absolute vorticity), and f_0 (the Coriolis parameter).

The static stability parameter γ is defined as

$$\gamma = \left(\frac{d\ln T}{d\ln P}\right)_{\text{adi}} - \frac{\partial \ln T}{\partial \ln P},$$

where $(d\ln T/d\ln P)_{\text{adi}}$ is the ratio of the gas constant to the specific heat at constant pressure (the dry-adiabatic lapse rate) for dry processes, and is the moist-adiabatic lapse rate for saturated processes, while $\partial \ln T/\partial \ln P$ is the domain-averaged lapse rate.

REFERENCES

AAAS, 1979: Seasat mission overview. *Science,* **204,** 1405–1424.

Austin, J. M., 1947: An empirical study of certain rules of forecasting the motion and intensity of cyclones. *J. Meteor.,* **4,** 16–20.

Bosart, L. F., 1981: The President's Day snowstorm of 18–19 February 1979: A subsynoptic scale event. *Mon. Wea. Rev.,* **109,** 1542–1566.

Corbell, R. P., C. J. Callahan and W. J. Kotsch, 1976: *The GOES/SMS User's Guide.* National Environmental Satellite Service, NOAA, 118 pp.

Gerrity, J. F., Jr., 1977: The LFM model-1976: A documentation. National Oceanographic and Atmospheric Administration, Tech. Memo. NWS-NMC-60, 67 pp. [NTIS PB279-419].

Gray, W. M., and D. J. Shea, 1973: The hurricane's inner core region. II. Thermal stability and dynamic characteristics. *J. Atmos. Sci.,* **30,** 1565–1576.

Grube, P., 1979: Convection-induced temperature change in GATE. Colorado State University, Atmos. Sci. Rep. 305, 128 pp.

Hoffman, R. N., 1982: SASS wind ambiguity removal by direct minimization. *Mon. Wea. Rev.,* **110,** 434–445.

Holliday, C. R., and A. H. Thompson, 1979: Climatological characteristics of rapidly intensifying typhoons. *Mon. Wea. Rev.,* **107,** 1022–1034.

James, R. W., 1979: Anatomy of a storm. *Mar. Wea, Log,* **23,** 71–75.

Kesel, P. G., and F. J. Winninghoff, 1972: The fleet numerical weather central operational primitive equation model. *Mon. Wea. Rev.,* **100,** 360–373.

Leary, C., 1971: Systematic errors in operational National Meteorological Center primitive equation surface prognoses. *Mon. Wea. Rev.,* **99,** 409–413.

Maddox, R. A., 1980: Mesoscale convective complexes. *Bull. Amer. Meteor. Soc.,* **61,** 1374–1387.

NOAA, 1979: Smooth log, North Atlantic weather, September and October 1978. *Mar. Wea. Log,* **23,** 104.

Rasmussen, E., 1979: The polar low as an extratropical CISK disturbance. *Quart. J. Roy. Meteor. Soc.,* **105,** 531–549.

Reed, R. J., 1979: Cyclogenesis in polar air streams. *Mon. Wea. Rev.,* **107,** 38–52.

Sanders, F., 1971: Analytic solutions of the non-linear omega and vorticity equation for a structurally simple model of disturbances in the baroclinic westerlies. *Mon. Wea. Rev.,* **99,** 393–407.

——, and J. R. Gyakum, 1980: Synoptic-dynamic climatology of the "bomb." *Mon. Wea. Rev.,* **108,** 1589–1606.

Satyamurty, P., V. B. Rao and A. D. Moura, 1982: Subsynoptic-scale baroclinic instability. *J. Atmos. Sci.,* **39,** 1052–1061.

Shuman, F. G., and J. B. Hovermale, 1968: An operational six-layer primitive-equation model. *J. Appl. Meteor.,* **7,** 525–547.

Silberberg, S. R., and L. F. Bosart, 1982: An analysis of systematic cyclone errors in the NMC LFM-II model during the 1978–1979 cool season. *Mon. Wea. Rev.,* **110,** 245–271.

Staley, D. O., and R. L. Gall, 1977: On the wavelength of maximum baroclinic instability. *J. Atmos. Sci.,* **34,** 1679–1688.

Taubensee, R. G., 1978: Weather and Circulation of September 1978—a warm month in the middle of the country. *Mon. Wea. Rev.,* **106,** 1750–1757.

Tracton, M. S., 1973: The role of cumulus convection in the development of extratropical cyclones. *Mon. Wea. Rev.,* **101,** 573–593.

Weickmann, H. K., A. B. Long and L. R. Hoxit, 1977: Some examples of rapidly growing oceanic cumulonimbus clouds. *Mon. Wea. Rev.,* **105,** 469–476.